# IMAGE ANALYSIS AS A TOOL FOR SATELLITE-EARTH PROPAGATION STUDIES

Riza Akturan, Hsin-Piao Lin and Wolfhard J Vogel
Electrical Engineering Research Laboratory
The University of Texas at Austin
Austin, TX, 78758

## Abstract

Wc present a progress report on a useful new method to assess propagation problems for outdoors mobile Earth-satellite paths. The method, Photogrammetric Satellite Service Prediction (PSSP), is based on the determination of Land Mobile Satellite Systems (LMSS) service attributes at the locations of static or mobile LMSS service users by evaluating fisheye images of their environment. This paper gives an overview of the new method and its products.

## Introduction

All personal satellite communications systems (S-PCS), whether targeted for vehicular or personal usc and whether operating at UHF, L-, S-Band or higher frequencies 19, 20, 21], are ultimately performance limited by onc of three basic propagation states [22]. The line-of-sight signal may bc (1) clear, (2) shadowed by trees, or (3) blocked by solid objects, i.e. buildings and mountains. Measurement campaigns to establish a propagation database for systcm simulation and performance prediction using real or simulated satellite transmissions arc very time-consuming and expensive. Thus, a more cost-effective method of determining the probability of the three transmission states is needed.

Previous field mcasurerncnts [1, 22, 23] have demonstrated a statistical link between fading and the three-state description of signal propagation. This research [2, 4] expands on that viewpoint with measurements with a system that evaluates full images of the upper hemisphere and determines where the sky is clear, where it is shadowed by vegetation, and where it is blocked as illustrated in Figure 1. Assuming that enough images are acquired in a specific environment, one can develop statistics for the three fade states as a function of elevation and azimuth angles [3, 5, 6] and these can bc combined with state-dependent propagation data to produce realistic simulated data or fade statistics [9].

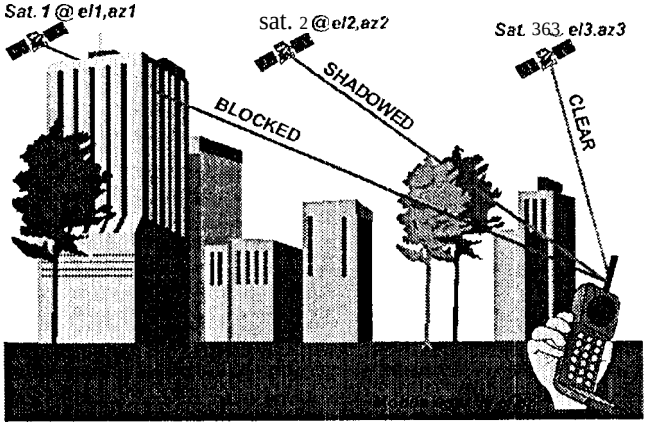


Figure 1. LMSS communication channel illustration.

There are a number of reasons why this method works: ( 1 ) Propagation effects for S-PCS are imposed by the physical environment within a short range from a mobile user terminal. (2) The propagation paths are elevated and thus permit visual inspection along their near-termina] extent from the mobile's location. (3) The statistical properties of the received signal levels can be described by a few, physically reasonable distributions which are a function of the fade state. (4) Suitable parameters for the distributions at frequency bands of interest have already been determined by many measurement campaigns.

Hence, provided that the propagation parameters arc known for an LMSS service environment, a generalized description of signal propagation is possible when conditioned on path states, and the path states can bc readily obtained from optical mcasuremcnts. This idea permits the cost-effective prediction of service availability in a specific area without the need for ncw RF measurements [9]. The method is especially effective in (1) predicting fading

probability as a function of elevation angle, (2) path (a.k.a. satellite) diversity gain, or (3) good-call durations for a specific constellation at a given latitude, all in a chosen environment.

In photogrammetric analysis, still and video images of the sky are taken through a fish-eye lens with a 180° field-of-view. Efficient image processing algorithms implement a three-state classification of the fisheye lens images. Using the products of image processing, two- and three-state environment statistics are derived by determining the skyline and three-state fractions in the classified images. This image data is applied to derive the elevation angle dependence of fading in LMSS channels. In addition, by placing satellite constellations on the images, time series of fading and Markov models of the communications channels are generated. From the time series, first order fade statistics are derived, and Markov models of the communication channel are prepared. Again, for the first time. an efficient procedure to derive satellite diversity gain and good-call durations by photogrammetry is introduced. In this text, satellite diversity gain is estimated extensively in urban, suburban and rural environments at different latitudes for different diversity operations. This derivation is performed for a diversity system that is able to operate a k-fold satellite signal combining scheme. Resulting time series of the diversity and non-diversity operations are also used in good-call duration calculations. In the following, this method and its products are presented in a logical order.

## Still and Video Image Processing

Our imaging system includes a fisheye lens, a HI-8 camcorder, a 35-mm still camera, a GPS receiver, a scanner, a video frame grabber, and VCR/TV units. Images are either 35-mm stills or 30 frame/second HI-8 videos of the sky taken with a camera through a fisheye lens having a 180° field-of-view, as shown in Figure 2A. Images are digitized and stored on a large capacity r nedium, typically a CD-ROM. In order to examine propagation characteristics of different environments, pictures are taken in urban, suburban or rural locations. Fisheye pictures are taken at the street-side of the sidewalks in the densely built areas and are taken on the roadsides in rural areas. Sampled locations include the USA, Canada and Japan.

The image processing system includes three steps [7, 8]. They arc pre-processing, state separation and state analyzing. Image processing starts with pre-processing of the digitized fisheye images. This involves two steps, north direction adjusting and unwrapping. When taking images, a GPS receiver is used to record the mobile vehicle's heading direction in a log. In processing, the fisheye images are rotated, using the log file, by the azimuth angle from north so that north always stay on the top. Later, image processing continues by unwrapping the images. Unwrapping, as shown in Figure 2B, converts from a circular image in which the zenith is at the center (o a rectangular coordinate system in which the zenith is at the top of the frame.

Next, still images are statistically analyzed using their selected spatial features [7]. The image processing system extracts vegetation and blockage features using search w indows in the images and evaluates these features to perform the thre.c-state classification in the regions defined by the corresponding search windows. To classify images, initially all image pixels are assumed as clear sky. When the total score of a search window feature density exceeds a threshold value, a state transition occurs; otherwise the pixel stays in the same state. This way, three-state images are obtained based on clear to blocked (Figure 2C) to shadowed (Figure 2D) sky transitions. Lastly, small objects are removed by erosion and dilation. To test the still image analysis algorithm, three-state fractions in urban Japan arc measured using automatically and manually classified images. The ratios of clear, shadowed, and blocked sky arc found as 58.7%, 4.4%, and 36.9%, respectively. Remarkably, the photogrammetric measurement results of the urban Japan images matched with field signal strength measurements [23]. As an error analysis, automatically classified images are compared with those classified manually using a paint program and mouse. The difference is assumed as the error measure of the image processing algorithm. The largest, 23%, and the lowest, 5%, state recognition errors arose in the urban and rural environments, respectively.

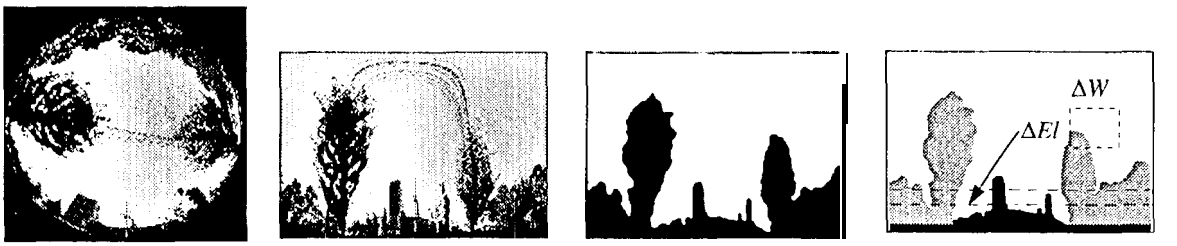


A. Fisheye Image B. Unwrapped Image C. Two-State Image D. Three-State Image

Figure 2. Still image analysis steps

Similarly, our video image processing technique [8] uses the RGB color palette as an object classification set to differentiate the image pixels into onc of three state types. Since the algorithm uses spatial image features in classification and only processes images that have changed since the last scene, the processing speed is vastly accelerated [8]. First, fisheye video images arc unwrapped, as explained previously. Second, key frames are extracted and t bird, using these key frames, fisheye videos are processed.

The implementation of the video image analysis procedure shows 80% clear, 14% shadowed and 4% blocked sky in a rural Los Angeles area. Processing errors are 7%, 5%, 4% in urban, suburban and rural Los Angeles environments, respectively. Figures 3A to 3B show the video image analysis steps, sample and processed fisheye images. In this image set, the gray regions correspond to the shadowing objects; the white regions correspond to the open sky. This specific image sequence dots not contain blockage objects.

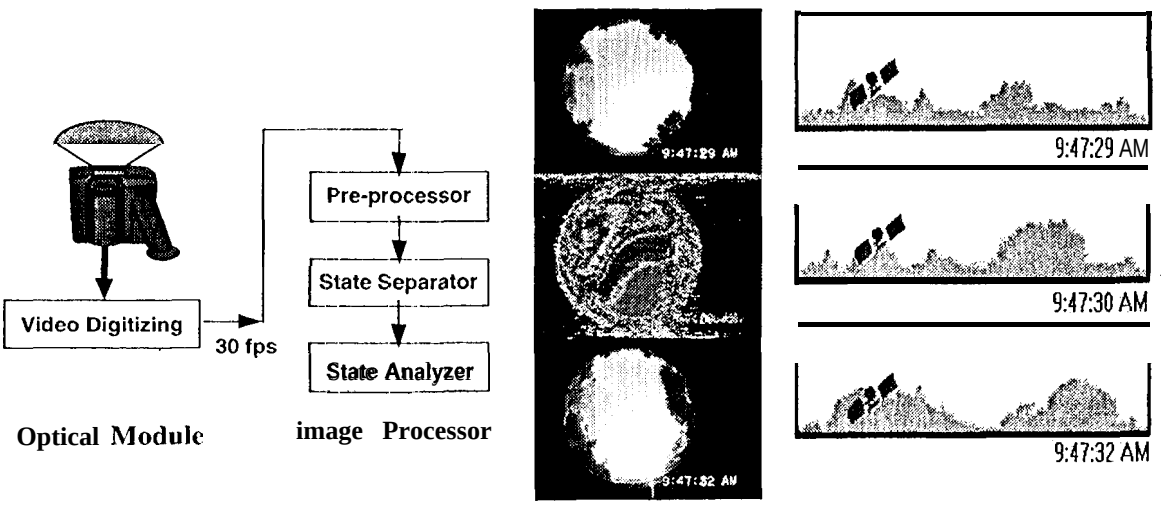


A. Image analysis system B. Sample video C. Analyzed video

Figure 3. Video image analysis steps

The programming and implementation have been done in C and C++ under a PC-Windows environment on a PC-586-90 platform. The effort has been directed towards developing reliable algorithms as well as minimizing processing speed [4]. An average video image analysis takes lcss than 5 s/image. Since the required size of the image data to bc stored is large compared to the size of available disk space, a lossless 4:1 compression scheme is developed and the compressed images are stored in a binary file [4].

In the fade state analysis, classified three-state images are read fi om the environment fade state tables as a function of azimuth and elevation. Classified three-state image resolution is 360x90 pixels, which presents a 1 'xl $^{0}$ resolution in mapping the environment.

## Environment Quantification Using Two-State Model: Skyline Statistics

In this section, results of two-state image processing arc presented. The fisheye images of four rural, suburban, and urban Texas locations are analyzed to derive quantitative information about the elevation

angles at which the sky becomes visible, i.e., the skyline [3, 6]. '1 'he mean skyline angle for an urban Austin image, Figure 4A, is shown in Figure 4B and the average histogram of skyline elevation angles shown in Figure 4C. Environment average skyline elevation angles in Austi n's rural, suburban and urban areas are 5°, 7°, and 26°, respectively. In the three environments, the 90'" percentile of the skyline was found to be at 11°, 17°, and near 55°, respectively.

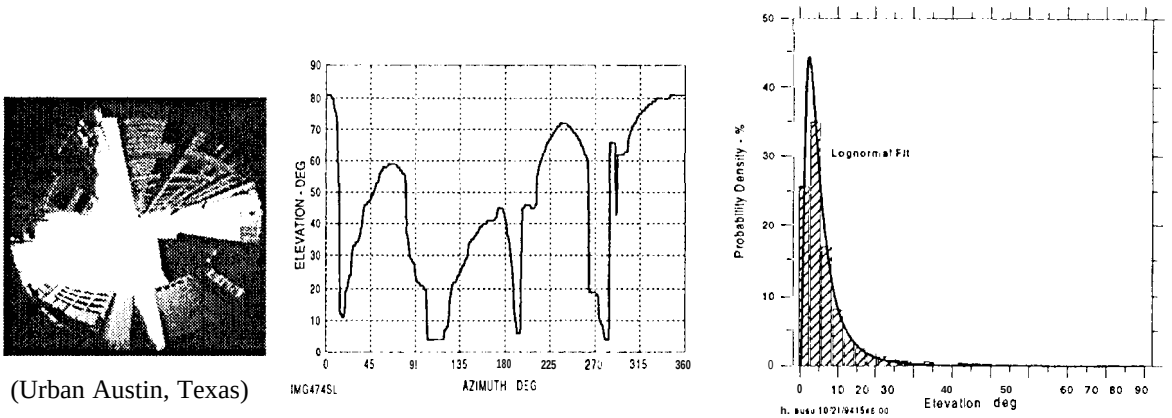


(Urban Austin, Texas)

A. Fisheye lens image B. Skyline C. Skyline elevation angles

Figure 4. Fisheye image of an urban Austin location, its skyline and skyline histogram

Above 10° elevation, on average 98% of the sky is visible in rural, 95% in suburban, 77% in urban Austin, and 68% in urban San Antonio as shown in Figure 5A. The potential of satellite diversity to mitigate tree-shadowing or blockage depends on the variability and structure of the skyline with azimuth at any particular location and on the satellite constellation. The $10^{th}$ percentile, mean, and $90^{th}$ percentile of the skyline autocorrelation in all three environments decreases to l/e with a lag of about 15°, 30°, and 55°, respectively. The skyline autocorrelations in Figure 5B have a similar shape in all environments. The autocorrelations cross zero near 70° azimuth lag. The median autocorrelation falls to zero near 50°, meaning that for half the locations in urban Austin there is an even chance that at 50° satellite separation the second satellite. will be clear if the first one is blocked (or the converse).

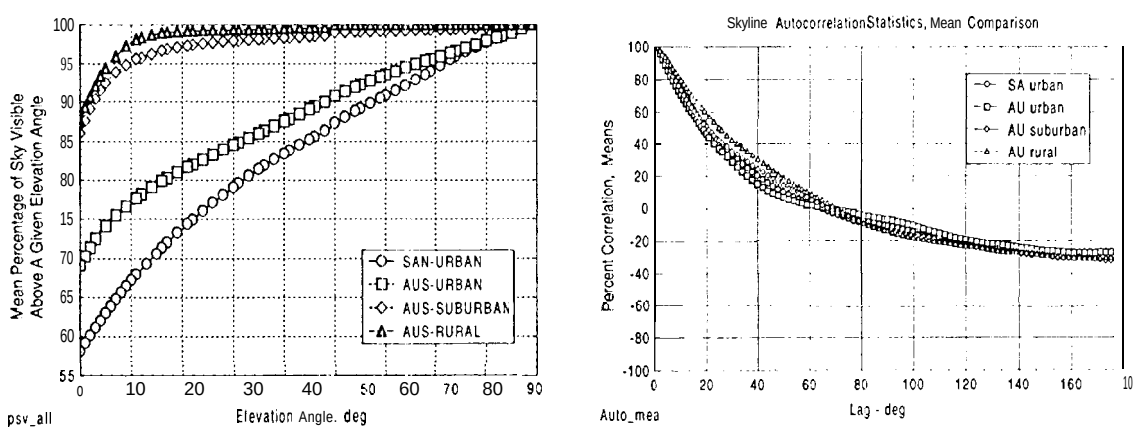


A. Sky visible ratios above given elevations B. Means in skyline autocorrelations

Figure 5. Skyline visibility and autocorrelation statistics

## Environment Quantification Using Three-State Model

Until now, environments have been defined verbally such as heavily or lightly shadowed. In this section, an environment quantification method is presented. Using ternary descriptions of environments, three-state

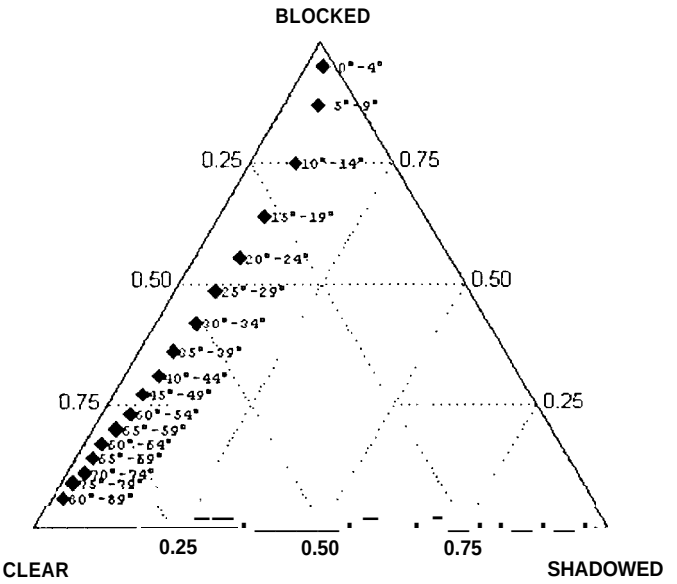


Figure 6. A ternary graph of propagation states in urban Japan as a function of the elevation angle in 5 degree increments.

images, environments were mapped onto environment triangles as illustrated in Figure 6, so that a quantitative ternary description of the environments was obtained [12].

Using the images of urban Japan, the fraction of potential satellite paths with clear, shadowed, or blocked line-of-sight was calculated in 5° elevation angle increments from 0° to 89° [10, 11]. The result has been plotted in Figure 6 in the form of a ternary graph. It is obvious that blockage as opposed to shadowing is of primary importance in the urban environment and that with decreasing elevation less of the sky is clear. For example, in the low-elevation interval from 10° to 14°, 17% of the sky is clear, 8% is shadowed, and 75% is blocked, compared against the higher elevation interval of 60° to 64°, where the state mixture $\vec{M}$ equals (0.8, 0.03, 0.17).

## Elevation Angle Dependence of LMSS Fading

Combining each path state derived from images for single or multiple satellites in a specific constellation with frequency-appropriate statistical fade models allows predicting overall performance measures such as fade dependence with elevation angle or path diversity gain [12,14]. Using the three-state method, for the first time, elevation dependence of fading is derived [10, 11]. In addition, the importance of including specular reflections under urban blockage conditions is established with an urban three-state signal distribution model [12].

Fisheye images of urban Japan were analyzed to derive, as a function of elevation, the fraction of sky that is clear, shadowed by trees, or blocked by buildings. At 32" elevation, the path state vector matches that derived from satellite measurements fit to a 3-state fade model [10]. Using, the same model, for the first time the elevation angle dependence of mobile satellite fading is predicted [10,11]. 'l-he dominance of building blockage fading in urban areas is expressed in the terracing of the cumulative distribution. It is found that in the Rayleigh domain, the minimum elevation with 90% coverage decreases by about 5" per dB of additional fade margin [11 ].

Heuristically, each of the three. possible path states of a mobile satellite link can be associated with a distinct fade distribution as expressed in this text. The *clear* state is usually described by a Ricean distribution, which represents the superposition of a line-of-sight (LOS) signal with multipath reflections, but neglects specular effects. The *shadowed* state was modeled by Loo [24] as a combination of a lognormally attenuated line-of-sight signal with Rayleigh distributed diffusely scattered power, and in the *blocked* state only Rayleigh distributed diffusely scattered power is considered.

$$f_v(v) = C \cdot f_{Rice}(v) + S \cdot f_{Loo}(v) \cdot B \cdot f_{Rayleigh}(v) \quad (1)$$

Furthermore, the importance of including specular reflections from nearby illuminated building surfaces under urban blockage conditions is added. This study improved on the model's fit by including potential specular reflections in the blocked state and by refining the distribution parameter estimates. To acknowledge the presence of such specular reflections, the distribution in the urban blocked state was changed from Rayleigh to Loo, resulting in the *urban* 3-state model

$$f_v(v,\alpha) = C(\alpha) \cdot f_{Rice}(v) + S(\alpha) \cdot f_{Loo}(v) \cdot B(\alpha) \cdot f_{Loo}(v) \quad (2)$$

Including specular reflections in the blocked state reduces the rms modeling error (right ) from about 1.3 dB to 0.5 dB as shown in Figure 7.

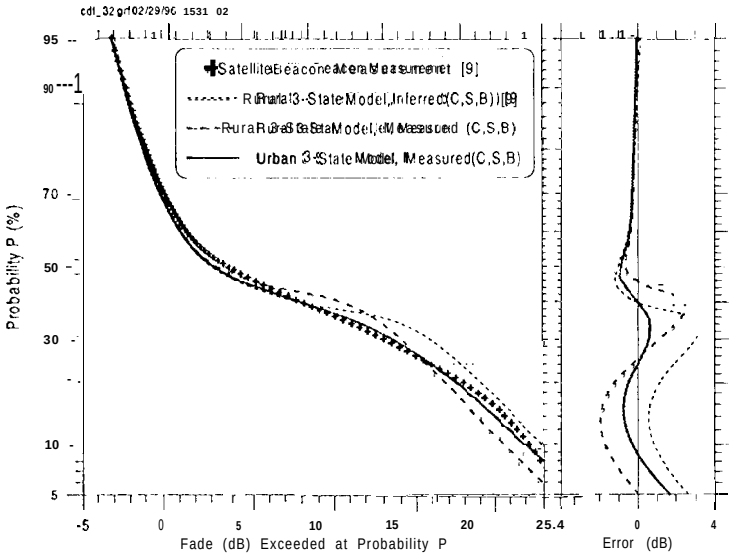


Figure 7. Comparison of a CDF measured in urban Japan at 32° elevation with three 3-state models.

Fade CDFs for urban Japan at elevation angles from 7° to 82°, based on photogrammetrically dctcrmincd path states and the urban 3-state fade probability model, ar shown in Figure 8. Photogrammetry permitted the prediction of fading as a function of the path elevation angle, and simple ternary plots are used to estimate non-diversity fading as a function of the path state vector. In urban Japan, it is found that the required fade margin decreases by about 0.2 dB/degree, from 25.5 dB to 15 dB at the 10% probability level and in the elevation range from 12° to67° [13, 14].

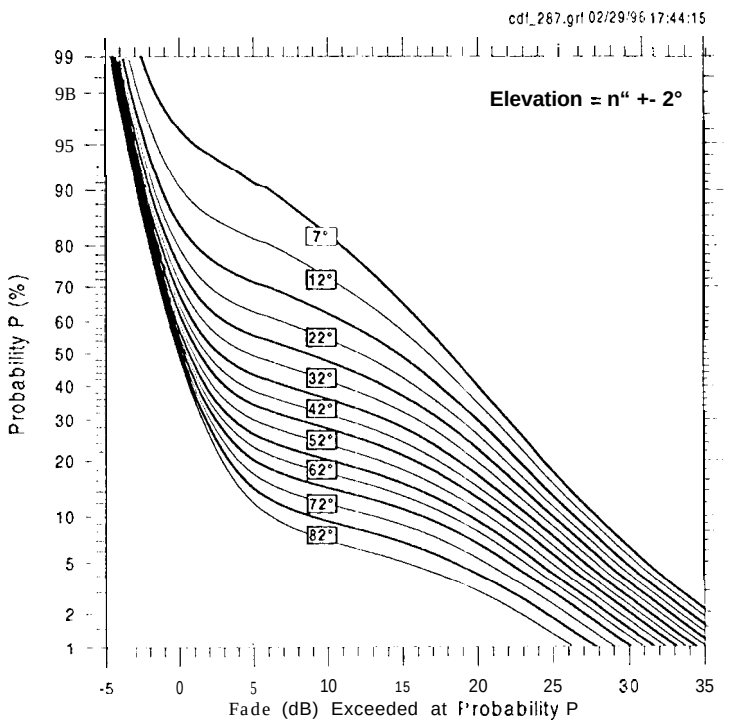


Figure 8. Fade CDFS for urban Japan

# Received Signal Generation

The system presented in this section substitutes video image processing for propagation measurements and permits flexible fade simulation of Land Mobile Satellite Communication systems [15]. The video image processing system is used to track the propagation states of the satellites in selected environments. The path state tracking is then applied to generate a satellite to mobile unit path state sequence as a time series. Analyzing sequences of images resulted in a propagation state time series which is input to a channel simulators shown in Figure 9. By assuming that the channel attributes are quasi-static in each propagation state [22], the statistical models are represented by Rayleigh for urban, Loo's for shadowed and Ricean for open direct LMSC paths. Using these state-specific propagation statistics, a time series of the received signal envelope is generated from the time series of the produced state sequences. The simulated signal time series are subsequently used to derive the first order propagation statistics of the communication channel [15].

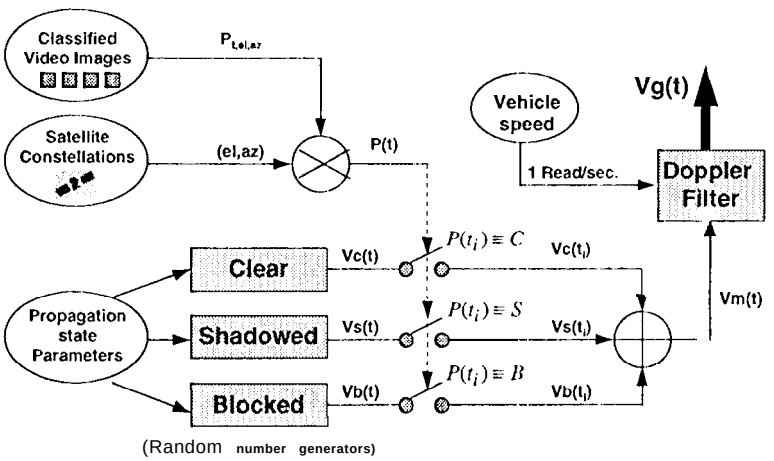


In simulation, a one-minute section of a video clip taken in suburban Pasadena is processed. A comparison of the fade series obtained by simulation and by measuring 2055 MHz cw transmissions from a TDRS satellite at 210 elevation and 249° azimuth in Pasadena, CA is shown in Figure 10, right graph. The rms difference between the two PDFs is 0.11. This close match shows the effectiveness of the photogrammetric procedure.

Figure 9. Received signal generation procedure

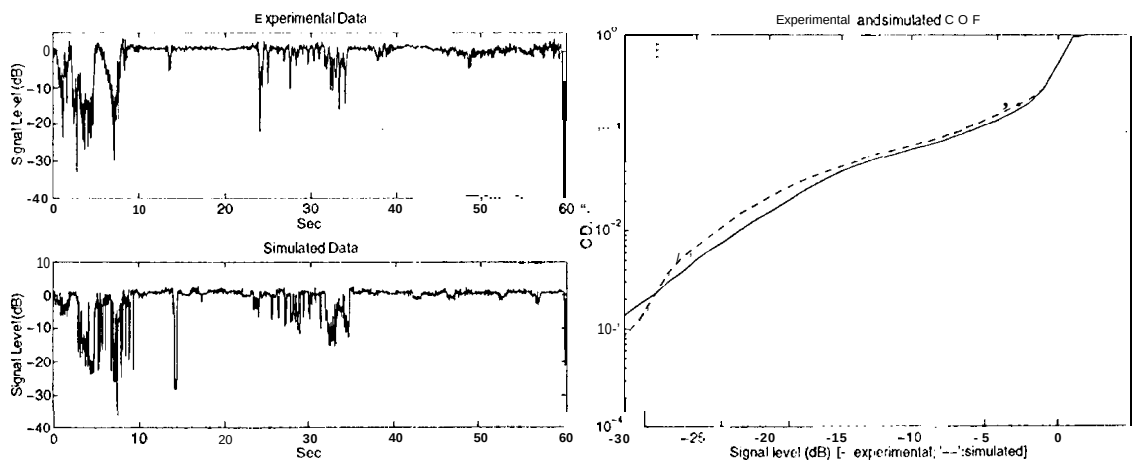


Figure 10. One minute time series of the measured and simulated signals and C.D.F. of one minute data

In a typical LMS scenario, while the mobile unit is in motion, the field strength of the received signal level changes with respect to the time and space according to the changing morphology of the environment. It has been shown [25] that the switching between different attenuation levels can be represented as a Markov stochastic process using the assumption that the channel properties are quasi-stationary in small time periods. Based on this propagation modeling method, our image processing and propagation channel simulation algorithms are employed to obtain a statistical representation of the communication channel [4]. The video image processing system is capable of tracking the propagation state of the path to any satellite in the selected environment, generating a satellite to MES path state sequence time series. Using random

number generators and the state sequences as shown in Figure 11, the received signal levels are predicted based on the state transition probabilities represented by Markov chains [ 16, 17, 18].

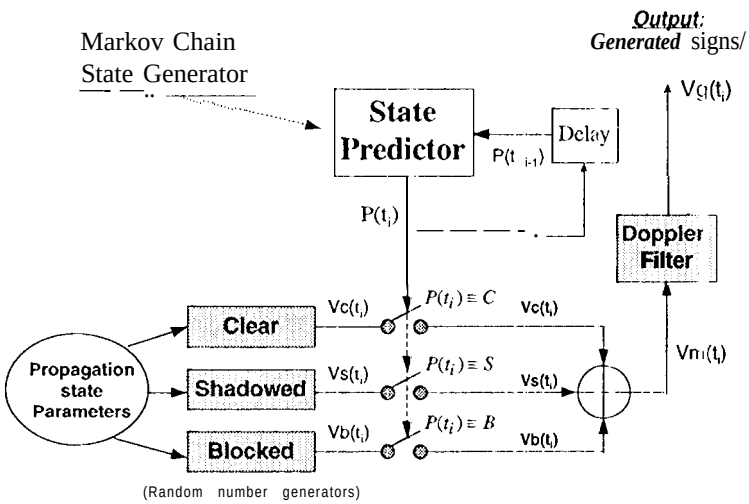


Figure 11. Signal generation using Markov chains

The simulation procedure was applied to the above two-minute section of simultaneous satellite fade data and video clip taken in suburban Pasadena, CA. Using the previously described procedures, the path state sequences, transition matrices and modeling parameters were found in the selected environments for thresholds $T_1$=-2.5dB and $T_2$=-20dB.

Comparisons of the simulated fade time series with measured data are shown in Figure 12. Because these time series are generated using the Markov method with state and transition probabilities derived from the entire two minutes of data, there is no one-to-one correspondence with the measurements.

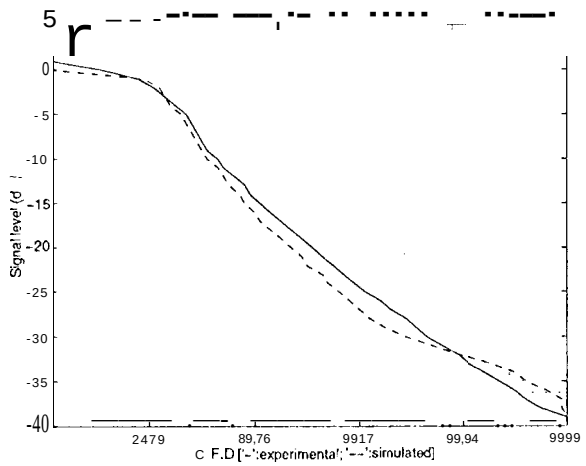


Figure 12. CDF of the suburban Pasadena data

The signal level first and second order statistics, i.e., the cumulative fade distribution (CDF) and level crossing rate (LCR) agree, however. The rms normalized difference between measured and simulated cumulative level probabilities is 2.5% and the rms normalized LCR error in Hz is 3.7 for wooded Pasadena. The best match of the CDFS is obtained in the suburban environment, where the state transitions occurred with regularity throughout the measurement and at a moderate rate that could easily be followed in the video images. Related state duration and transition Markov matrices are given in Figure 13 with a diagram of the Markov process.

As described, fisheye image sequences are used to generate the received signal levels. A sample of the software is shown in Figure 14 to illustrate this process [4]. A Windows-based program processes the fisheye images and extracts states. Then, using the statistical signal distributions in respective states, signal levels are generated as a function of time.

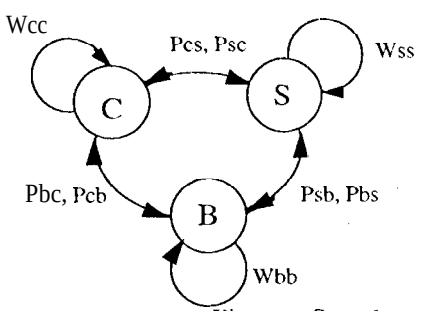


State. duration Matrix:
W := (0.7522 0.2142 0.0336)

State Transition Matrix:

$$P := \begin{pmatrix} 0.9815 & 0.0166 & 0.0018 \\ 0.0597 & 0.9170 & 0.0233 \\ 0.0413 & 0.1488 & 0.8099 \end{pmatrix}$$

Figure 13. State durations and transitions in suburban Pasadena, CA

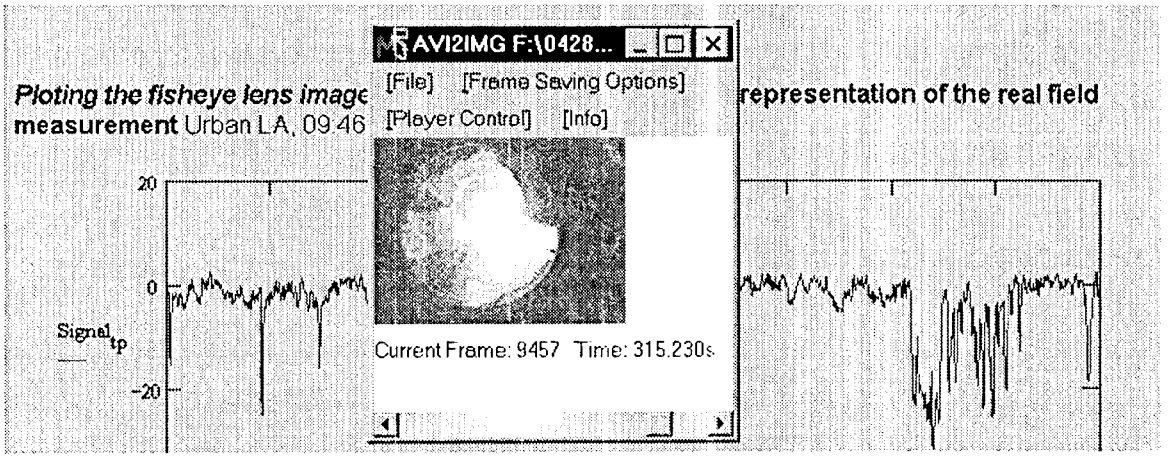


Figure 14. Signal generation software

## Satellite Diversity Gain

For the first time [12, *14],* diversity gain statistics are estimated for LEO satellite PCS. An image processing procedure to track the visible satellite path states is developed. The diversity gain estimation involves a 4-fold path diversity scheme with k from one to four, where the best k satellites are used in the link [12]. The calculation of *k-fold* diversity gain involves 4 steps: (a) determining the CDFs according to coherent combining: $v = v_1 + v_2 + .. + v_k$ and switching combining: $v = \max(v_1, v_2, .., v_k)$, (b) placing the satellite constellation into the 3-state images and determining the probability of occurrence for each state combination, (c) summing all CDFs from step (a) weighted by the probabilities of step (b), and (d) subtracting the resulting CDF from the CDF of the highest satellite at the same city at probabilities from 1% to 99%.

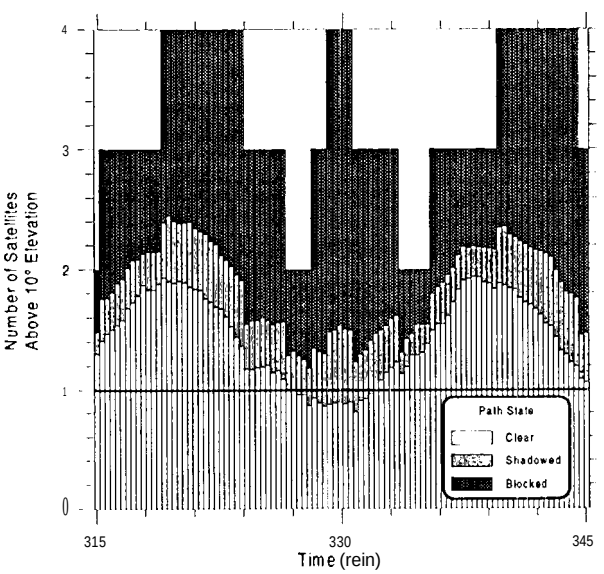


Figure 15. The image-average number of satellites

Stacked bar graphs for 30 minutes of the image-averaged number of satellites visible with (from bottom to top) *clear*, *shadowed,* and *blocked* path states are depicted in Figure 15 for a Globalstar-like constellation, 48 satellites on 8 planes, in Tokyo. The number of *clear* satellites varies periodically between <1 and <2 and most of the time three or four satellites are available. The minimum elevation angle was 10°.

By employing this procedure, satellite diversity gain of any satellite communication system is estimated without actually using any satellites. Measurements have shown that satellite diversity increases availability of the communication channel by introducing, more satellites in clear paths. However, satellite diversity gain greatly depends on the constellation's orbiting characteristics. Path diversity gain for combining and hand-off diversity is found for up to *4-fold* diversity at a high-, mid- and low-latitude location for the sample constellation. With *2-fold* or higher order diversity, it is near 10 dB and 6 dB at probabilities below 20% when using two or more satellites in the non-equatorial and equatorial locations, respectively.

Figure 16 shows coherent combining path diversity for the Globalstar-like constellation in Tokyo that reduces fading relative to using the highest satellite. Fading at 10% probability, for instance, can be reduced from above 20 dB to below 1() dB by combining signals from as many as four satellites.

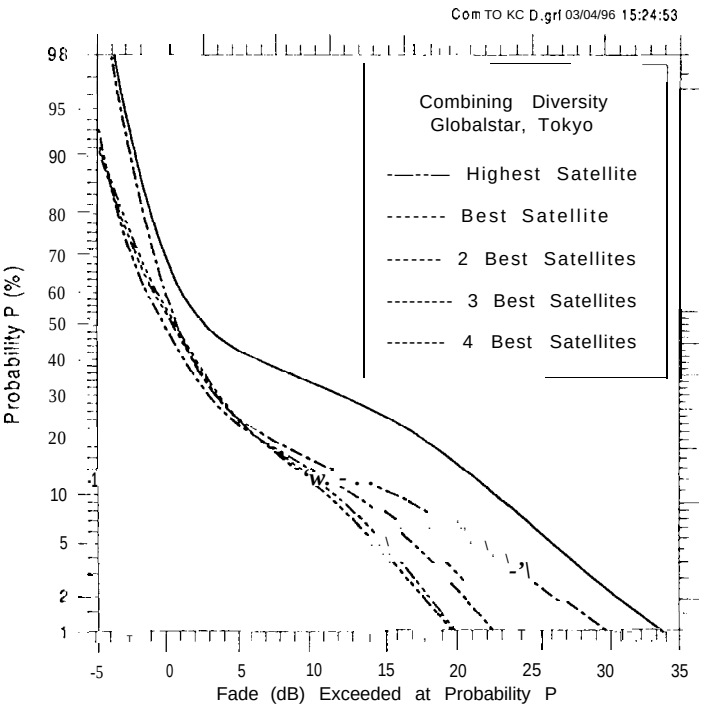


Figure 16. Coherent combining path diversity

Figure 17 shows a comparison of path diversity gain achieved by combining (thick lines) and hand-off (thin lines) diversity with up to four satellites of the Globalstar constellation in Tokyo. Gains for both methods are equal when using the best satellite, but with more satellites combining diversity achieves greater gain.

Figure 18 shows a service comparison between the four environments for the service coverage of 98%, 95%, **90%** by receiving signal from only the highest satellite or the two best satellites using hand-off diversity. Using this setup, at 95% coverage, the improvement obtained by using the two best satellites instead of the highest is 9 dB, 9 dB, 6 dB and 3 dB in urban Austin, urban San Antonio, suburban Austin and rural Austin. The two urban environments show similar fade characteristics. As it can be seen clearly, non-diversity fading in a suburban environment is lower than diversity fading in an urban environment. This shows that satellite diversity is mostly valuable in urban environments although it decreases fading in suburban and rural environments. The path diversity gain in mid- and low- probabilities are almost half of the diversity gain in urban Austin.

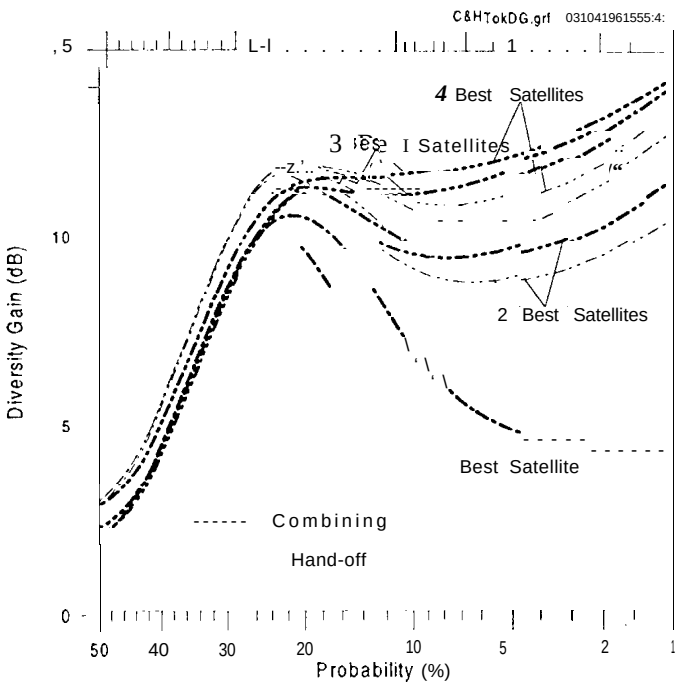


Figure 17 Comparison of combining, and hand-off diversity

As a result of the photogrammetric method, it is observed that satellite diversity is useful in providing an adequate link margin [4]. It increases availability of the communication channel and lowers the need for high satellite elevation angles. Diversity gain strongly depends on the constellation's orbit parameters. Large azimuth separations between the visible satellites and a high standard deviation in the average elevations of the visible satellites result in a high diversity gain, recalled from above. Diversity gain is high in heavily shadowed or blocked environments. According to the environment dcpcndcnce plots [4], a

3 dB/environment gain increase is estimated from the combining diversity gain values that arc 10 dB, 7 dB and 4 dB in urban, suburban and rural Austin, respectively.

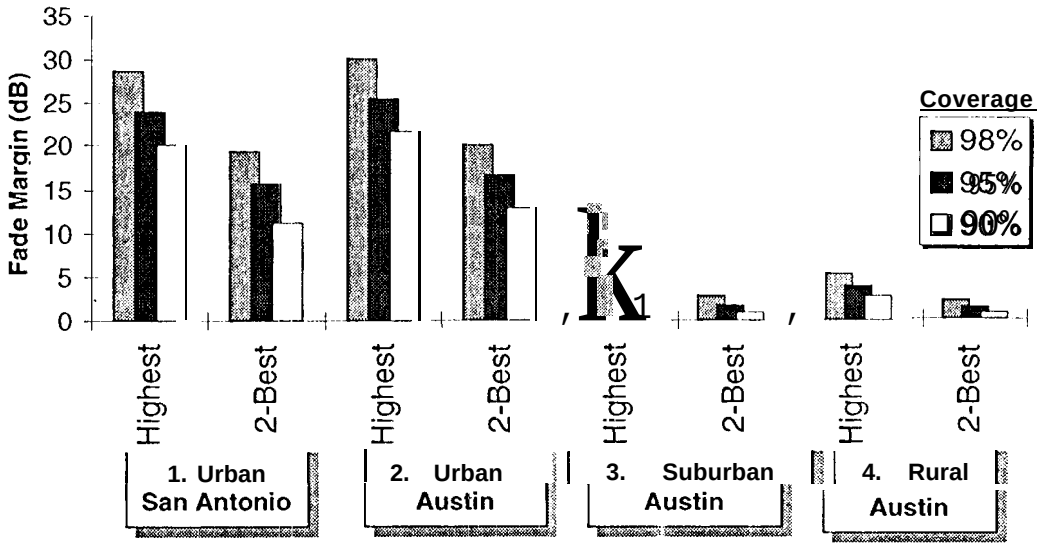


Figure 18 Comparison of path diversity gain using combining diversity with four satellites in Austin, TX.

## Communication Channel Stability: Good Call Durations

Similar to [26], a good-call duration analyzer is derived from the diversity analysis procedure [4]. The procedure places the satellite constellations on the classified images [ 12]. Later, for each time sample, the best satellite and the highest satellites arc chosen, and their states are determined as a function of time. The states for these two satellites are written into a state-log file. One log file for the best satellite (non-diversity operation) and onc log file for the highest satellite (diversity operation). Then, using a math package, state durations are examined.

A good state or channel occurs when the line of sight (LOS) signal can be transmitted for the duration of the call. Conversely, a bad state or channel occurs when the LOS signal can not bc transmitted for 18 sec. A bad state causes interruption in signal transmission, and the current call is dropped. To implement this method, it is assumed that the good state occurs when the LOS is clear, when there arc no obstructions in the direct path from a mobile or fixed user to the satellite. Therefore, the clear state durations are tracked and call-completion success is

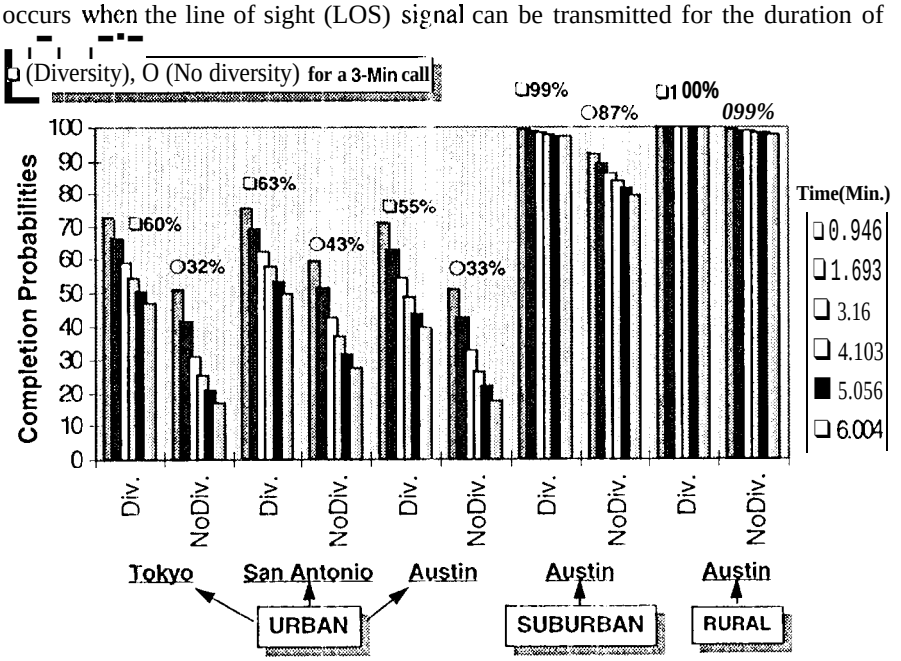


Figure 19. Good-call durations in different environments

calculated using the above procedure. The results are derived using a Globalstar-like constellation without considering specific system parameters and implementations.

As Figure. 19 suggests, 60% and 35% of the three-minute calls are successful] y completed without an 18 sec channel interruption using diversity and non-diversity operations, respectively, in the three urban environments. These numbers go up to 99% and 100% in suburban and rural environments, respectively, with diversity operation. The rural environment without diversity supports a call completion probability of around 99%, whereas in the suburban environment without diversity operation it drops 12% down to 87910.

# Conclusion

As a result of this work, derivation of a ternary description for clear, shadowed and blocked path states allowed one to combine satellite orbit design with propagation statistics to predict performance such as fade probability or diversity gain in a specified environment. Photogrammetry is a new tool with which one can derive service predictions for personal and mobile satellite communications systems in any environment. It is inexpensive and simple compared to other techniques. The data collection process does not require receiving a signal from a satellite or other platform, and results can be applied to any frequency band for which statistical fade parameters are available. The products of photogrammetric satellite service prediction should be of immediate use to satellite system designers. The method opens new capabilities of propagation prediction for Land Mobile Satellite Communication Systems. A milestone table is given in Figure 20.

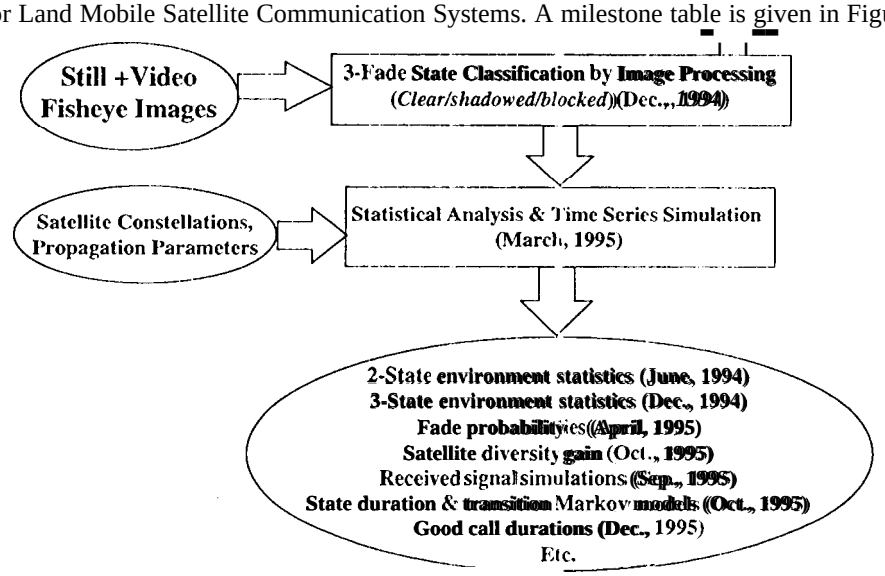


Figure 20. Photogrammetric measurement system architecture with the completion times of its steps.

# Bibliography


[1] Birdwell, B., "*Design of an optical sensor system to replicate the effects of signal blockage and shadowing on satellite signs 1 propagation,*" M.S. Thesis, The University of Texas-Austin, Austin, Texas, May 1993.

[2] Akturan, R. and Vogel, W.J., "Photogrammetric Mobile Satellite Service Prediction," *Proc. of the Eighteenth NASA Propagation Experiments Meeting, NAPEX XVIII,* Vancouver, BC Canada, June 16-17, 1994.

[3] Akturan, R. and Vogel, W. J., "Photogrammetric Mobile Satellite Service Prediction," *Project Report, Submitted to Jet Propulsion Laboratory of NASA,* Pasadena, CA, Nov. 1, 1994.

[4] Akturan, R., "Photogrammetric Mobile Satellite Service Prediction," Ph.D. *Dissertation proposal, Submitted to the Graduate School of the University of Texas-Austin, Nov. 17, 1994.*

[5] Akturan, R. and Vogel, W. J., "Photogrammetric Mobile Satellite Service Prediction," *National Academy of Sciences and Engineering Meeting, URSI'95,* Boulder, CO, Jan. 3, 1995, p 210.

[6] Akturan, R. and Vogel, W. J., "Photogrammetric Mobile Satellite. Service Prediction," ***Electronic Letters***, Feb. **2, 1995, vol. 31, No. 3, p 165.**

**[7]** Akturan, R. **and** Vogel, W.J., "classification of Attenuation Sources In Satellite PCS Using Image Processing," *Proceedings of the Signal and Image Processing Conference*, Las Vegas, NV, Nov 20, 1995.

[8] Akturan, R., Hudson, F. and Vogel, W. J., "A Fast Video Image Processing Technique For Tracking Attenuating Objects in Satellite Communication Paths," *Proceedings of the Second Joint Conference on Information Sciences,* Wrightsville, NC, Sep.28, 1995.

[9] Akturan, R, Lin, H.P. and Vogel, W.J., "Elevation Angle Dependence of Fading for Satellite PCS in Urban, Suburban and Rural Environments," *National Academy of Sciences and Engineering Meeting,* Boulder, CO., Jan. 9, 1996.

[10] Akturan, R. and Vogel, W. J., "Elevation Angle Dependency of Fading for Satellite PCS in an Urban Area," *Electronic Letters*, July 1995, vol. 31, No. 14, pp. 1125-1127.

[11 ] Akturan, R. and Vogel, W. J., "Optically Derived Elevation Angle Dependence of Fading For Satellite PCS," *Proc. of the 19th NASA Propagation Experiments Meeting, NAPEX XIX,* Fort Collins, CO, June 14, 1995.

[12] Akturan, R. and Vogel, W. J., "Path Diversity for LEO Satellite-PCS in the Urban Environment," *Project Report, Submitted to Jet Propulsion Laboratory of A'ASA,* Pasadena, CA, Dec. 13, 1995.

[13] Akturan, R. and Vogel, W. J., "A Method to Derive Satellite Diversity, " *National Academy of Sciences and Engineering Meeting, URSI'96*, Boulder, CO, Jan. 9, 1996.

[14] Akturan, R. and Vogel, W. J., "Path Diversity for LEO Satellite-PCS in the Urban Environments" *Submitted to IEEE Trans. on Antennas and Propagation.*

*[15]* Akturan, R., Lin, H. I'. and Vogel, W.J., "Propagation Modeling In Land Mobile Satellite Sytems Using Photogrammetry," *Proc. of the IEEE Vehicular Technology Conference '96,* Atlanta, GA, April 28, 1996.

[ 16] Lin, H. P., Akturan, R. and Vogel, W.J., "Propagation Channel Simulation for LMSS and Satellite PCS," *National Academy of Sciences and Engineering Meeting, URSI'96*, Boulder, CO, Jan. 9, 1996.

[17] Lin, H. P., Akturan, R. and Vogel, W. J., "Photogrammetric Satellite PCS Channel Modeling Using Markov Chain Approach," *Proc. of the International Conference on Communications'96*, Dallas, TX, June 23, 1996.

[ 18] Lin, H. P., Akturan, R. and Vogel, W. J., "Satellite-PCS Channel Simulation in Mobile User Environments Using Photogramrnetry and Markov Chains," *Submitted to Special Selected Papers Issue in Communications, ACM/Baltzer Wireless Information Networks (WINET).*

[ 19] Schindall, J., "Concept and implementation of the Globalstar Mobile Satellite System", *Proceedings of the Fourth International Mobile Satellite Conference,* Ottawa, Canada, June 6-8, 1995.

[20] Tadano, H., "IRIDIUM- a Lockheed Transition to Commercial Space", *Proceedings of the Fourth international Mobile Satellite Conference,* Ottawa, Canada, June 6-8, 1995.

[21 ] Sturza, M., "Architecture of The Teledesic Satellite System," *Proceedings of the Fourth International Mobile Satellite Conference,* Ottawa, Canada, June 6-8, 1995.

[22] Goldhirsh, J. and Vogel, W. J., "Propagation Effects for Land Mobile Satellite Systems: Overview of Experimental and Modeling Results," *NASA Reference Publication 1274,* February 1992.

[23] Karasawa, Y., Minamisono, K. and Matsudo, '1'., "A Propagation Channel Model For Personal Mobile-Satellite Services," *Proc. 1994 Progress in Electromagnets Research Symp., ESA*, (Noordwijk, The Netherlands). 11-15 July, 1994.

[24] Loo, C., "A Statistical Model for a Land Mobile Satellite Link," *IEEE Trans. on Vehicular Technology,* vol. 34, no. 3, pp. 122-127, Aug. 1985.

[25] Vucctic, B., and Du, J., "Channel Modeling and Simulation in Satellite Mobile Communication Systems," *IEEE Journal on Selected Areas In Communications*, Vol. 10, No. 8, Oct. 1992.

[26] Penwarden, K., "Propagation Model for LEO Satellites," *URSI* '96, *National Academy of Sciences and Eng. Meeting,* Boulder, CO., Jan. 9, 1996.